A Neural Network Based Landing Method for an Unmanned Aerial Vehicle with Soft Landing Gears

Cai Luo [1,*] **, Weikang Zhao** [1] **, Zhenpeng Du** [2] **and Leijian Yu** [3]

[1]   College of Mechanical and Electronic Engineering, China University of Petroleum (East China), Qingdao 266580, China

[2]   School of Petroleum Engineering, China University of Petroleum (East China), Qingdao 266580, China

[3]   Department of Design, Manufacture & Engineering Management, University of Strathclyde, Glasgow G1 1XJ, UK

*   Correspondence: luo_cai@upc.edu.cn

check for updates

Abstract: This paper presents the design, implementation, and testing of a soft landing gear together with a neural network-based control method for replicating avian landing behavior on non-flat surfaces. With full consideration of unmanned aerial vehicles and landing gear requirements, a quadrotor helicopter, comprised of one flying unit and one landing assistance unit, is employed. Considering the touchdown speed and posture, a novel design of a soft mechanism for non-flat surfaces is proposed, in order to absorb the remaining landing impact. The framework of the control strategy is designed based on a derived dynamic model. A neural network-based backstepping controller is applied to achieve the desired trajectory. The simulation and outdoor testing results attest to the effectiveness and reliability of the proposed control method.

Keywords: unmanned aerial vehicle; neural network; soft landing gear

1. Introduction

Unmanned aerial vehicles (UAVs) in human-unreachable environments have aroused great interest in the civil, military, and engineering fields [1–3]. Within the group of drones, quadrotor helicopters have gained increasing interest, due to their maneuverability, simple structure, affordability, and agility. Information about the use of UAVs can be obtained from a number of new publications, with topics ranging from earthquake searching to the deployment of air-dropped goods for humanitarian purposes [4–6]. Furthermore, for missions such as delivering first-aid supplies, drones always need ground support, such as airports or landing stations. However, outside cities and bases, UAVs may quite easily encounter the situation that there is no suitable landing assistance infrastructure nearby [7–9]. This will severely limit the usability of drones.

Flying animals, such as birds, can perch on trees, poles, and other non-flat surfaces which are not suitable for UAV landing. Equipped with this soft landing ability, birds may occupy a high vantage point [10]. They can stay there to search, forage, and rest for an extended period of time [11,12]. As a high-challenge landing approach, perching refers to precise landing pose control and the effectiveness of energy absorption [13]. Cory and Tedrake, of the MIT Computer Science and Artificial Intelligence Laboratory, have analyzed and presented fixed-wing precise drone landing tests and demonstrated that angles of attack are critical factors during the touchdown procedure [14]. Mirko Kovac from the Imperial College of London designed an aerial robot equipped with soft shock absorbers which can land on a convex surface with diameter longer than robot's body length [15]. Subsequently, many inspired mechanical devices have been investigated to test this hypothesis. For example, a pitch-up touchdown sequence, consisting of distance detection, UAV nose up, and soft

contact with a landing zone, has been proposed by Stanford University [16,17]. A passive micro-spine grapple was proposed for perching under tree branches [18].

UAVs are, at present, continue to be sent out to achieve safety, security, and rescue missions. Numerous robust control schemes have been developed to address the control problems in quadrotor helicopters associated with uncertainties and delays. In [19], a dynamic model of a quadrotor helicopter with a suspended payload was established, and a non-linear controller, without considering the parametric uncertainty, was also presented. In [20], a switching model predictive controller was proposed for the rejection of external disturbances. In [21], the author presented a feedback linearization control approach by considering the disturbance from the payload. To maintain the posture tracking performance against external uncertainties, an H_∞ theory-based approach was proposed in [22]. As an alternative method, the sliding model control technique was used in [23] to reduce the parameter variation effect on the closed-loop control system. In addition, a quadrotor transportation platform involves time-varying delays. In [24], constant state delays were analyzed within the quadrotor helicopter system. The input delays to the system were further discussed in [25]. In [26–28], radial basis function neural network (RBFNN)-based PID controllers were proposed to control quadrotor flying robots without separating the inner loop and the outer loop. However, the multiple non-linear uncertainties and disturbances were not considered in the design approach, which has a sub-optimal impact on the performance of UAVs.

With the demand to land on a non-flat surface, this paper demonstrates the design and fabrication of a novel quadrotor helicopter system. The proposed platform uses a backstepping theory-based flight controller working with a neural network algorithm, which enables a drone to safely land on a non-flat platform. In this paper, a non-linear flight controller is proposed. First, a RBFNN approach is employed, in order to address the unknown disturbances. Second, the disturbances in the position and pose control input are suppressed with the modified neural network-based methodology. Third, the stability of the proposed control approach is proven through Lyapunov stability analysis. Finally, the RBFNN-based nonlinear controller is verified by real-time outdoor experiments.

The main three contributions of this paper are as follows:

- The design of a novel elastomer landing gear is achieved. It guarantees safe landing on a convex surface with diameter smaller than the quadrotor body length through a conventional vertical landing strategy.
- A neural network-based backstepping technique is adopted to meet the desired vertical landing requirement, and soft landing is achieved using the proposed controller with near-zero landing speed. The stability of the landing control system is proved through the Lyapunov approach and the backstepping technique.
- The proposed platform is challenged in a real flight outdoor scene, which validates the controller's effectiveness and robustness.

This paper is organized as follows. Section 2 introduces the modeling of the UAV and soft elastomer landing gear. In Section 3, we introduce the landing control algorithm and stability analysis. The simulation of the quadrotor helicopter landing is discussed in Section 4. The prototype of the UAV and real-world outdoor setup used to assess the control method are demonstrated in Section 5. Finally, the conclusion and future work are discussed in Section 6.

2. Quadrotor Modeling and Landing Gear Architecture

The quadrotor helicopter used in this work is shown in Figure 1. The structure of this UAV is in cross mode. The quadrotor helicopter can be considered a rigid, cross-shaped frame bearing four motors and propellers. The center of mass (COM) is set to coincide with the geometric center of the quadrotor's body. The attitude and altitude of the quadrotor helicopter can be controlled by changing the speed of each rotor. As shown in Figure 1, Rotors 1 and 3 rotate clockwise, while Rotors 2 and 4 rotate anticlockwise [29–31].
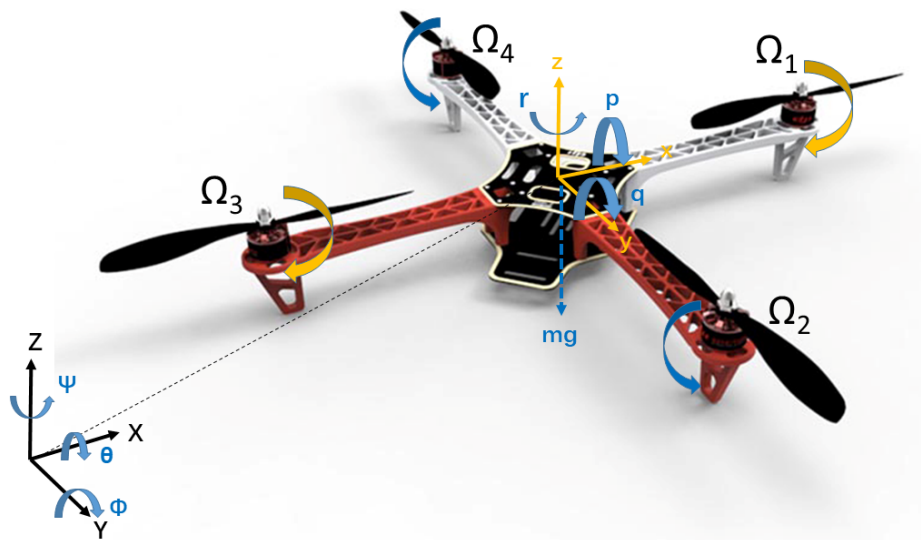
Figure 1. A cross-type quadrotor helicopter.

2.1. The Modeling of the Quadrotor Helicopter

According to the formalism of Newton–Euler approach, the quadrotor dynamics can be expressed as [32]:

$$\ddot{x} = (\cos\phi \sin\theta \cos\psi + \sin\phi \sin\psi)\frac{u_1}{m} + D_x$$

$$\ddot{y} = (\cos\phi \sin\theta \sin\psi - \sin\phi \cos\psi)\frac{u_1}{m} + D_y$$

$$\ddot{z} = (\cos\phi \cos\theta)\frac{u_1}{m} - g + D_z$$

$$\ddot{\phi} = \dot{\theta}\dot{\psi}\frac{I_y - I_z}{I_x} + \frac{J_r}{I_x}\dot{\theta}\Omega_r + \frac{l}{I_x}u_2 + D_\phi \qquad (1)$$

$$\ddot{\theta} = \dot{\psi}\dot{\phi}\frac{I_z - I_x}{I_y} - \frac{J_r}{I_y}\dot{\phi}\Omega_r + \frac{l}{I_y}u_3 + D_\theta$$

$$\ddot{\psi} = \dot{\phi}\dot{\theta}\frac{I_x - I_y}{I_z} + \frac{1}{I_z}u_4 + D_\psi,$$

where (x, y, z) is the position of the center of the gravity of the UAV in the earth-frame; (p, q, r) denotes the angular velocity in the body-frame; m is the total mass of the UAV; g is the gravity acceleration; l represents the arm length of UAV; the moments of inertia are represented by Ix, Iy, and Iz, respectively; ϕ, θ, and ψ are the roll, pitch, and yaw Euler angles; J_r denotes the moment of inertia; D_x, D_y, D_z, D_ϕ, D_θ, and D_ψ represent the uncertain disturbances; $\Omega_i (i = 1, 2, 3, 4)$ is the ith propeller speed; and $\Omega_r = \Omega_1 - \Omega_2 + \Omega_3 - \Omega_4$ is the overall speed of propellers.

2.2. The 3D Schematic and Modeling of the Soft Landing Gear

As presented in Figure 2, a soft passive gear is fixed under the quadrotor helicopter to facilitate landing impact absorption. The requirements for this end-effector include:

- The ideal touchdown velocities and posture of the quadrotor helicopter.
- Suitable mechanical and material properties of the landing gear to absorb the high-speed impact force to protect the body of the UAV, as seen in Figure 3.
- To fulfill the requirements for drones to achieve successful touchdown, the landing structures must meet the need to absorb the impact forces during the landing contact.

Figure 2. The 3D schematic of the proposed quadrotor helicopter.

The Elastosil M4601 silicone material that was used to fabricate the soft landing gear has hyper-elastic properties. The ABAQUS package was used to simulate the impact displacement and the reactions of the soft landing gear. In the simulation, the coefficients of strain energy were set as C10 = 0.11 and C20 = 0.02. The density was set as 1130 kg/m^3.

The coordination system of the landing gear is shown in Figure 4. In the simulation, the upper part of the gear was allowed to move in the *x–z* plane, while the lower part was allowed to rotate around the *x*-axis. The impact load was added to the upper part of the gear along the *z*-axis. Figure 3 demonstrates the maximum displacement of the soft landing region when encountering different impact forces (5 N, 10 N, 15 N, 20 N, and 25 N).
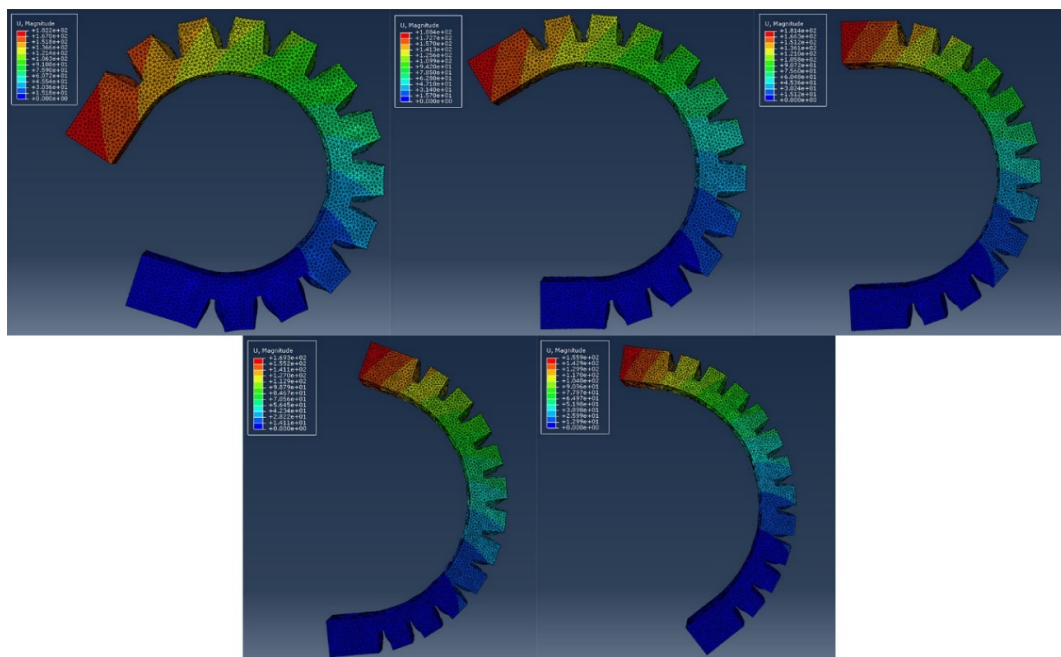

Figure 3. The maximum displacement of the soft landing region when encountering different forces.
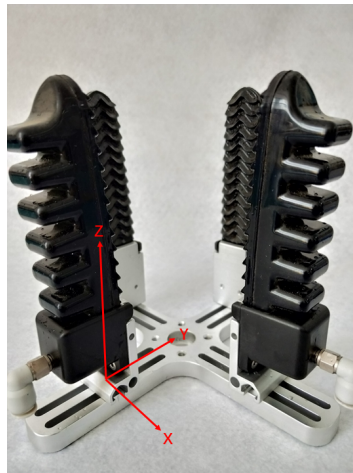
Figure 4. The proposed soft landing gear.

3. Controller Design and Stability Analysis

As shown in Figure 5, the control system of the proposed quadrotor contains two loops: An outer loop and an inner loop. The PID control method in the outer loop is used for the position and altitude control, while the exploited RBFNN-based control approach is implemented in the inner loop for stable attitude control.
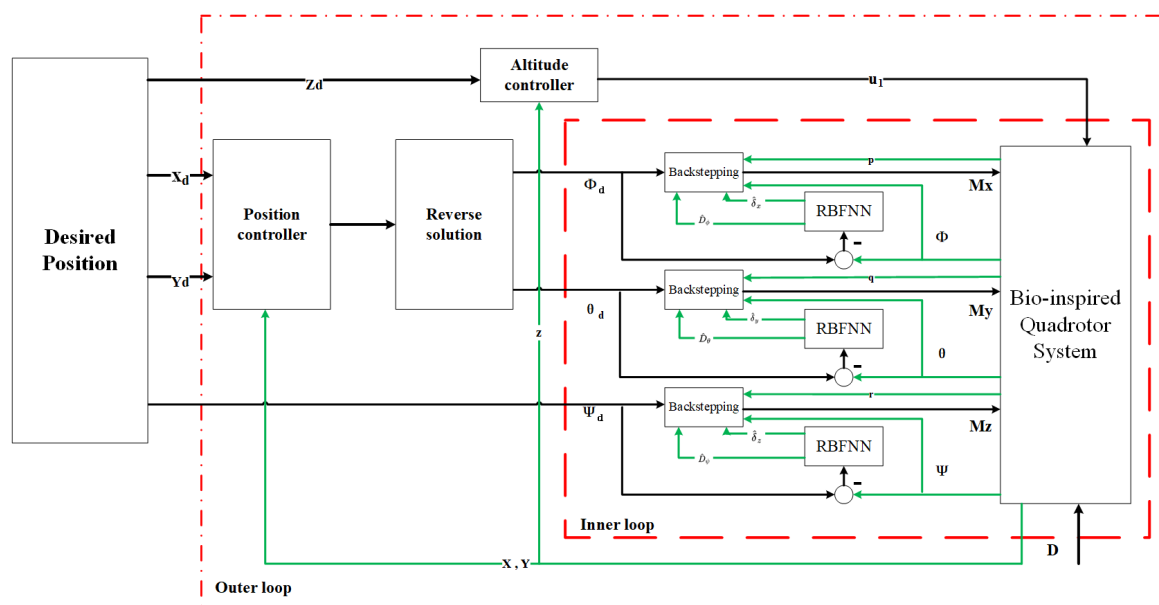

Figure 5. The control block diagram of the proposed approach.

3.1. PID Position and Altitude Control Design

P_z is the PID controller of UAV altitude in the z direction, which is defined as

$$P_z = K_{zP}\left(z_d - z\right) + K_{zI} \sum_{i=1}^{k} t_s \times \left(z_{di} - z_i\right) + K_{zD}\left(\dot{z}_d - \dot{z}\right), \tag{2}$$

where K_{zP}, K_{zI}, and K_{zD} are the proportional, integral, and differential coefficients in the controller, respectively, and t_s is defined as the time step.

P_x and P_y are the PID controller of the UAV position in the x–y plane, which are defined as

$$
\begin{aligned}
P_x &= K_{xP}\,(x_d - x) + K_{xI}\sum_{i=1}^{k} t_s \times (x_{di} - x_i) + K_{xD}\,(\dot{x}_d - \dot{x}) \\
P_y &= K_{yP}\,(y_d - y) + K_{yI}\sum_{i=1}^{k} t_s \times (y_{di} - y_i) + K_{yD}\,(\dot{y}_d - \dot{y}).
\end{aligned}
\tag{3}
$$

The desired attitude angles (roll and pitch) can be derived as

$$
\begin{aligned}
\phi_d &= -\arctan\left(\frac{P_y}{P_z + g - D_x}\right), \\
\theta_d &= \arctan\left(\frac{P_x}{P_z + g - D_x}\right).
\end{aligned}
\tag{4}
$$

3.2. RBFNN-Based Backstepping Attitude Control Design

Attitude control using the adaptive RBFNN-based backstepping control method is shown in inner loop of Figure 5. The attitude control of the quadrotor helicopter is controlled by three different inputs (roll, pitch, and yaw). The attitude control in roll, pitch, and yaw have the same design procedure in the proposed control method. For the sake of simplicity, we only take the roll channel as the example design process to describe in this section.

The roll channel is denoted as

$$
\begin{aligned}
\dot{x}_1 &= x_2 \\
\dot{x}_2 &= \frac{M_x}{I_x} + D_\theta,
\end{aligned}
\tag{5}
$$

where x_1 is the roll angle and x_2 denotes the derivation of x_1.

The external disturbance is denoted, by D_θ, as

$$
D_\theta = \Xi_x + \varpi_x,
\tag{6}
$$

where $\Xi_x = \Delta M_x / (I_x + \Delta I_x)$ denotes the external bounded disturbance and $\varpi_x = -\Delta I_x M_x / [I_x(I_x + \Delta I_x)]$ is treated as the model uncertainty.

The tracking error of roll angle is defined as [33]

$$
e_1 = x_{1d} - x_1,
\tag{7}
$$

where x_{1d} is the desired roll angle.

Then, the derivative of e_1 is

$$
\dot{e}_1 = \dot{x}_{1d} - x_2.
\tag{8}
$$

The first Lyapunov function is chosen as

$$
V_1 = \frac{e_1^2}{2}.
\tag{9}
$$

The tracking error of roll angle velocity is defined as

$$
e_2 = x_2 - \dot{x}_{1d} - c_1,
\tag{10}
$$

where the stabilizing function c_1 is defined as

$$
c_1 = \alpha e_1,
\tag{11}
$$

where α is a positive constant.

Thus, the derivative of V_1 can be obtained by

$$
\dot{V}_1 = e_1\,(\dot{x}_{1d} - x_2) = -e_1 e_2 - \alpha e_1^2.
\tag{12}
$$

Then, the derivative of e_2 can be represented as

$$
\begin{aligned}
\dot{e}_2 &= \dot{x}_2 - \ddot{x}_{1d} - \alpha\dot{e}_1 = \\
&\frac{M_x}{I_x} + D_\theta - \ddot{x}_{1d} + \alpha\left(e_2 + \alpha e_2\right).
\end{aligned}
\tag{13}
$$

The assosicate Lyapunov function is denoted as

$$
V_2 = V_1 + \frac{1}{2}s^2,
\tag{14}
$$

and the related sliding surface is designed as

$$
s = ke_1 + e_2,
\tag{15}
$$

where k is a positive constant.

The derivation of V_2 can be obtained by

$$
\begin{aligned}
\dot{V}_2 &= \dot{V}_1 + s\dot{s} \\
&= -e_1 e_2 - \alpha e_1^2 + s\left(k\dot{e}_1 + \dot{e}_2\right) \\
&= -e_1 e_2 - \alpha e_1^2 + s\left[(k-\alpha)\dot{e}_1 + \frac{M_x}{I_x} + D_\theta - \ddot{x}_{1d}\right].
\end{aligned}
\tag{16}
$$

3.3. RBFNN-Based Observer

In real-world outdoor applications, the bound for the uncertainty D_θ in the roll channel is hard to estimate. Considering this, we chose an adaptive RBFNN observer to adapt the estimated the uncertainty value $\hat{D}_\theta$ in the UAV system. The chosen RBFNN was a three-layer feed-forward neural network [34,35].

The vector in the input layer is $Z = [e_1, \dot{e}_1]^T$. By using the weighted sum method, the output is derived as follows

$$
\begin{aligned}
\hat{D}_\theta &= \sum_{j=1}^{N} W_j \phi_j(\mathbf{Z}), \quad j = 1, 2, \cdots, N \\
\phi_j(\mathbf{Z}) &= \exp\left(-\frac{\|\mathbf{Z} - M_j\|^2}{\sigma_j^2}\right)
\end{aligned}
,
\tag{17}
$$

where W_j denotes the connective weight, N is the number of hidden nodes, M_j is the centre vector, and the positive scalar σ_j denotes the spread width. The receptive field function uses a Gaussian function in our designed neural network.

3.4. Stability Analysis

The minimum reconstructed error σ_x is defined in the roll channel as

$$
\sigma_x = D_\theta - \hat{D}_\theta\left(\mathbf{W}^*\right),
\tag{18}
$$

where $\mathbf{W}^*$ represents an optimal weight vector in the approximation.

Then, an associated Lyapunov function is chosen as

$$
V_3 = V_2 + \frac{\zeta_1}{2}\left(\mathbf{W}^* - \mathbf{W}\right)^T\left(\mathbf{W}^* - \mathbf{W}\right) + \frac{\zeta_2}{2}\left(\delta_x - \hat{\delta}_x\right)^2,
\tag{19}
$$

where ζ_1 and ζ_2 are defined as positive constants, and $\hat{\delta}_x$ denotes the approximated value of the minimum reconstructed error; δ_x is provided to compensate the observed error induced by the RBFNN uncertainty observer.

Then, the derivation of the Lyapunov function V_3 is obtained as

$$
\begin{aligned}
\dot{V}_3 &= \dot{V}_2 - \zeta_1 \left(\boldsymbol{W}^* - \boldsymbol{W}\right)^{\mathrm{T}} \dot{\boldsymbol{W}} - \zeta_2 \left(\delta_x - \hat{\delta}_x\right) \dot{\hat{\delta}}_x = \\
&\quad - e_1 e_2 - \alpha e_1^2 + s \left[(k - \alpha)\dot{e}_1 + \frac{M_x}{I_x} + D_\theta - \ddot{x}_{1d}\right] - \\
&\quad \zeta_1 \left(\boldsymbol{W}^* - \boldsymbol{W}\right)^{\mathrm{T}} \dot{\boldsymbol{W}} - \zeta_2 \left(\delta_x - \hat{\delta}_x\right) \dot{\hat{\delta}}_x.
\end{aligned}
\tag{20}
$$

Following the backstepping control law [36], U_x is equal to M_x, as

$$
U_x = M_x = I_x \left[-(k - \alpha)\dot{e}_1 + \ddot{x}_{1d} - \gamma s - h \operatorname{sgn}(s) - U_H - U_R\right],
\tag{21}
$$

where γ and h denote positive constants, and U_H and U_R are designed as the robust and compensated controllers, respectively. They are denoted as shown in Equation (22)

$$
\begin{aligned}
U_H &= \hat{D}_x(W), \\
U_R &= \hat{\delta}_x.
\end{aligned}
\tag{22}
$$

The derivation of V_3 is obtained as

$$
\begin{aligned}
\dot{V}_3 &= -e_1 e_2 - \alpha e_1^2 - \gamma s^2 - h|s| + s \left[D_\theta - \hat{D}_\theta \left(\boldsymbol{W}^*\right) - \hat{\delta}_x\right] - \\
&\quad \zeta_2 \left(\delta_x - \hat{\delta}_x\right) \dot{\hat{\delta}}_x + s \left[\hat{D}_\theta \left(\boldsymbol{W}^*\right) - \hat{D}_\theta(\boldsymbol{W})\right] - \zeta_1 \left(\boldsymbol{W}^* - \boldsymbol{W}\right)^{\mathrm{T}} \dot{\boldsymbol{W}}.
\end{aligned}
\tag{23}
$$

Then, $\dot{V}_3$ can be rewritten as

$$
\begin{aligned}
\dot{V}_3 &= -e_1 e_2 - \alpha e_1^2 - \gamma s^2 - h|s| \\
&= -z^{\mathrm{T}} \Lambda z - h|s|,
\end{aligned}
\tag{24}
$$

where $z = \begin{bmatrix} e_1 & e_2 \end{bmatrix}$ and the symmetric matrix Λ is in the form

$$
\Lambda = \begin{bmatrix} \alpha + \gamma k^2 & \gamma k + \frac{1}{2} \\ \gamma k + \frac{1}{2} & \gamma \end{bmatrix}.
\tag{25}
$$

The adaptation laws for $\dot{\boldsymbol{W}}$ and $\dot{\hat{\delta}}_x$ are designed as

$$
\begin{aligned}
\dot{\boldsymbol{W}} &= \frac{s}{\zeta_1} \phi(\boldsymbol{Z}), \\
\dot{\hat{\delta}}_x &= \frac{s}{\zeta_2}.
\end{aligned}
\tag{26}
$$

According to Barbalat's lemma [37], it is noted that, when $\dot{V}_3 \leq 0$, Λ is guaranteed to be positive definite, as expressed by

$$
|\Lambda| = \gamma(\alpha - k) - \frac{1}{4} > 0.
\tag{27}
$$

Thereby, the roll state of the quadrotor UAV is asymptotically stable, based on the aforementioned condition. The other channels (pitch and yaw) control follow the same procedure, and are not described for the purpose of simplicity.

4. Simulation

In order to successfully land on a convex surface, the quadrotor needs to descend vertically to the landing target to avoid rolling over. The proposed RBFNN method will control the quadrotor in order to maintain straight attitude during the landing, under the conditions of external disturbances. The soft landing gear will demonstrate its ability to absorb the remaining impact force and help the quadrotor to perch on a convex surface, as shown in Figure 6.

Figure 6. Quadrotor successfully landed on convex surfaces with the support of the proposed soft landing gear.

To validate the real-time performance of the controller and assess the reliability and robustness of the proposed RBFNN-based backstepping control approach in the challenge of external disturbances, a Hardware-in-the-Loop (HITL) environment was developed for the UAV. The simulation platform was made up of two main parts: A hardware part and a software part. The hardware part was the Pixhawk autopilot unit, which was used in the field tests. The software part was the Matlab aerospace simulation environment. The hardware and software parts were connected by USB/UART to send and receive flight data. The RBFNN-based control approach was implemented by MATLAB 2018b and PX4 Autopilots Support from Embedded Coder.

The quadrotor helicopter model was used, for simulation validation, with the physical parameters listed in Table 1. The disturbances were added to the model by $\Xi = 0.3 \cos(0.2t)$ through an individual plugin. The RBFNN in the simulation used 2, 5, and 1 neuron(s) in the input, hidden, and output layers, respectively. The centre and width in Equation (17) were chosen as $m = 2$ and $\sigma = 6$, respectively. The coefficients ζ_1 and ζ_2 were chosen as 0.1 and 0.3, respectively. The parameters in Equation (25) were tuned by trial and error to achieve satisfying control performance, as shown in Table 2.

Table 1. Parameters of the quadrotor helicopter.

Symbol	Description	Value	Units
m	Mass	2	kg
l	Body length	450	mm
r	Rotor radius	100	mm
I_x	Moment of Inertia	1.85	10^{-3} kg $\cdot$ m^2
I_y	Moment of Inertia	1.85	10^{-3} kg $\cdot$ m^2
I_z	Moment of I nertia	2.98	10^{-3} kg $\cdot$ m^2

Table 2. Parameters of the backstepping sliding-mode control.

Parameter	Roll	Pitch	Yaw
α	11	14	12
k	0.4	0.4	0.3
γ	16	23	21
h	1.1	3.9	1.2

Five simulation tests were carried out to investigate the accuracy and repeatability of the proposed method, and the simulation path can be seen in Figure 7. The simulation steps were as follows:

1. The quadrotor started from an initial position $A(0, 0, 0)$.
2. The quadrotor flew to the position $B(2, 2, 6)$ and hovered there for attitude control tests; these results can be seen in Figure 8.
3. The quadrotor descended to the position $C(4, 2, 2)$ with a speed between 5–8 m/s.
4. The quadrotor, then, received the landing position $D(6, 2, 0)$. The UAV began to adjust its altitude, attitude, and velocity for the landing tests.
5. The quadrotor landed on the target without a high-speed impact.

In these tests, the numerical simulation demonstrates that all the quadrotor attitude states had a small steady-state error, subject to the external disturbance. As shown in Figure 8 and Table 3, the steady-state error was thoroughly eliminated in a short time using the RBFNN-based backstepping control method.

Table 3. Setting time and steady-state error in the hovering tests.

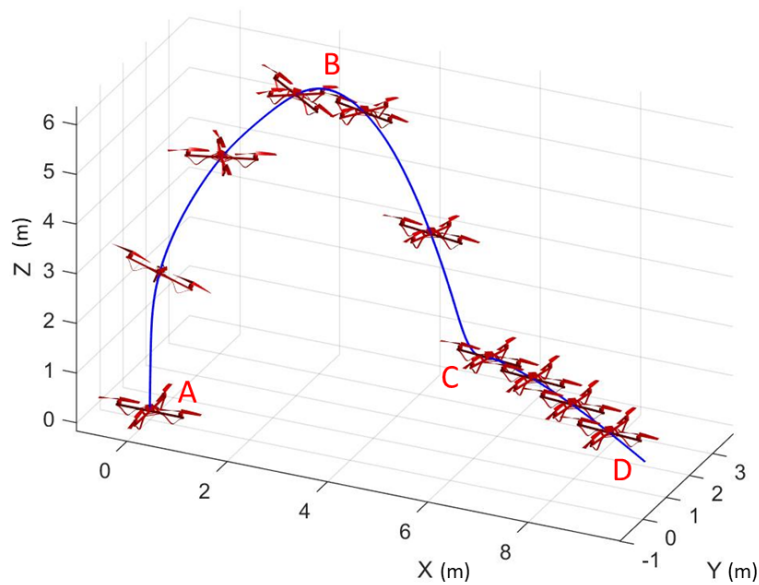| Attitude	Setting Time (s)	Steady-State Error (Degree)
Pitch	1.1	0
Roll	2.0	0
Yaw	1.1	0

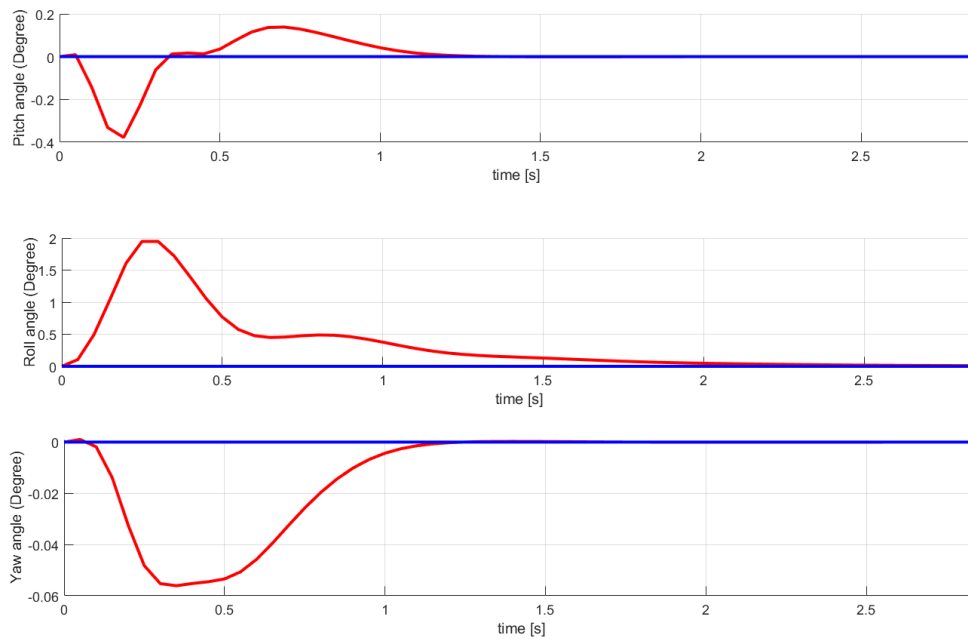**Figure 7.** Path and waypoints of the quadrotor in simulation tests.

Figure 8. Simulation curves of the quadrotor states in hovering stable tests.

Table 4 demonstrates the Root Mean Square Error (RMSE) of the touchdown position, related to the target surface position. From this, we can conclude that the goal-directed strategy could accurately control the quadrotor, which smoothly and precisely landed on the target (i.e., the velocity and distance both decreased to zero at almost the same time). Accordingly, the simulation results demonstrate that the proposed controller was capable of attaining satisfactory stable hovering and soft landing. Additionally, α can increase the response speed by adding to it's value, while huge increases in α will cause system instability. The steady-state error increases by reducing the value of k.

Table 4. Simulation landing position error.

RMSE Horizontal X,Y [m]	0.03
RMSE Vertical Z [m]	0.02

5. Outdoor Experiment of the Quadrotor with Soft Landing Gears

To further test the proposed control approach performance in the outdoor experimental situation. The system shown in Figure 9 is proposed to meet the requirements of non-flat surface landing tasks. The onboard devices include three units: The Flight Unit (FU), the Computing Unit (CU), and the Landing Gear (LG).
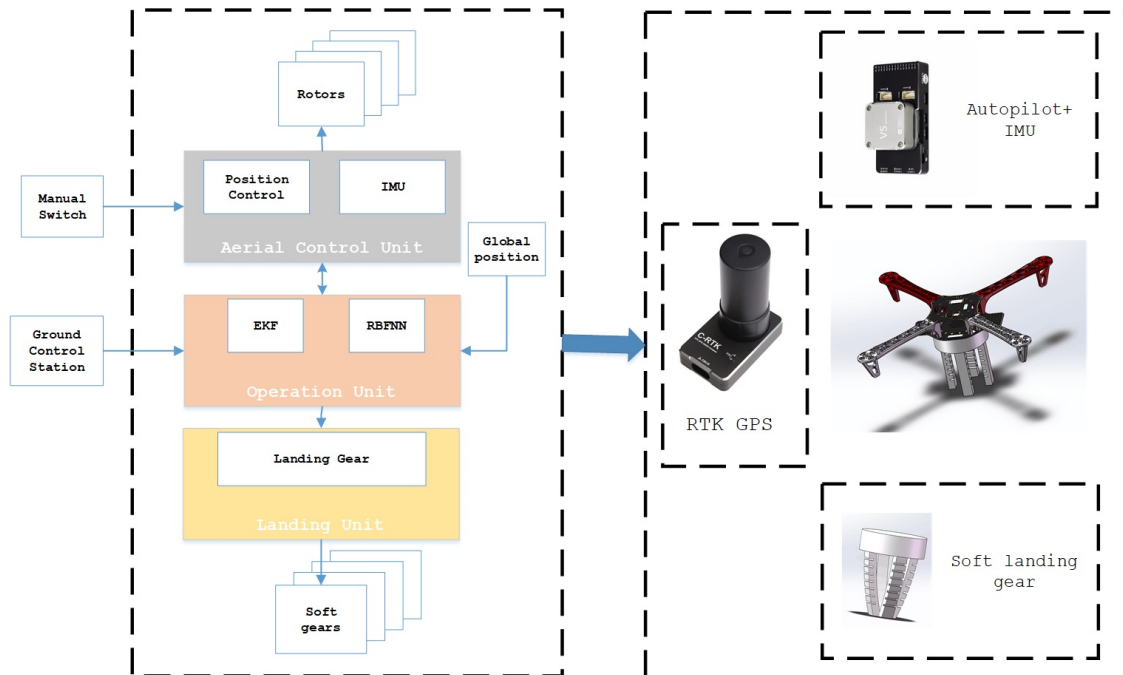
Figure 9. System structure of the quadrotor helicopter and the soft landing gear for the outdoor experiments.

The time-consuming complex tasks, such as path planning, GPS waypoint receiving, and manual switch engaging, are performed on the CU, which has an onboard processor. The position and altitude control are made on the FU. The FU receives speed values, hovering requirements, and landing tasks, sent from either the CU or from a human pilot equipped with remote controller (RC).

The integrated systems of the quadrotor helicopter are listed as follows:

- Flight System
  Autopilot devices: The onboard flight assistant device is a Pixhack-V5 flight autopilot board. The board is based on the Pixhawk open hardware design; it runs PX4 on the NuttX OS and is fully compatible with the PX4 firmware [38,39].
  Airframe: The structure of the quadrotor cross-shaped frame was built using polyvinyl chloride (PVC). The quadrotor UAV is equipped with four brushless DC motors and four Electronic Speed Controllers (ESCs).
  Attitude and altitude control: The 3D position is estimated by jointly using IMU and GPS.
  Communication Protocol: The communication link used onboard is the Mavlink protocol. The IMU and the onboard processor use this protocol to send command data [40]. The UAV and GCS are connected through a universal asynchronous receiver/transmitter (UART).
- Landing System
  Control devices: A PDMS-based four-finger soft landing gear mounted on the bottom the quadrotor body.

To evaluate the soft landing gear performance, twenty real field experiments were carried out in an open-space test field, as shown in Figure 10. The flight tests were performed under different weather conditions. The external wind speed was below 5 m/s. To date, the quadrotor helicopter with soft landing gear has successfully achieved stable landing on non-flat surfaces by using the proposed control approach.

During the tests in open space, there was always one pilot inspecting the state of the drone and one ground crew member monitoring the flight testing field. The ground crew was in charge of the

GCS. A human pilot took control over autopilot unit using the RC transmitter. Both personnel haD the option to send a full shutdown command to switch off all rotors immediately.

Figure 10. The proposed quadrotor helicopter system successfully landing on an outdoor non-flat surface with the support of the RBFNN controller.

During the experiments, the quadrotor helicopter attempted to land on a non-flat surface, as shown in Figure 10, which is common in real-world situations. In each of these 20 experiments, the propsosed quadrotor helicopter successfully landed on a non-flat surface without rolling over. Figure 11 displays the velocity, attitude estimation, and altitude over time in the landing process. Table 5 shows the RMSE of the touchdown position related to the desired position, where the vertical errors were generated by the quadrotor speeds decreasing to zero before solid contact with the surface.

Table 5. Field landing position error.

RMSE Horizontal X,Y [m]	0.07
RMSE Vertical Z [m]	0.06

Impact absorbing tests were implemented by controlling the quadrotor landing with different descent speeds (0.5 m/s, 1 m/s, 1.5 m/s, and 2 m/s). The relative landing accelerations were obtained by the Pixhawk accelerometer. The peak accelerations during the landing impacts were 21 m/s^2, 47 m/s^2, 96 m/s^2, and 194 m/s^2, respectively. Therefore, the impact forces that the soft landing gear encountered were 42 N, 94 N, 192 N, and 388 N, respectively. As demonstrated, the soft landing gear was fully capable of absorbing the landing impact without any damage to the structure of the UAV body. We also challenged the conventional rigid gear to land on a convex surface which was smaller than the quadrotor's body length. In these five challenges, none of them could successfully keep their balance on the surface and maintain a stable landing. According to the results, it is clear that the smooth and precise landing requirements of UAV were well-satisfied by the proposed RBFNN-based controller and soft landing gear.
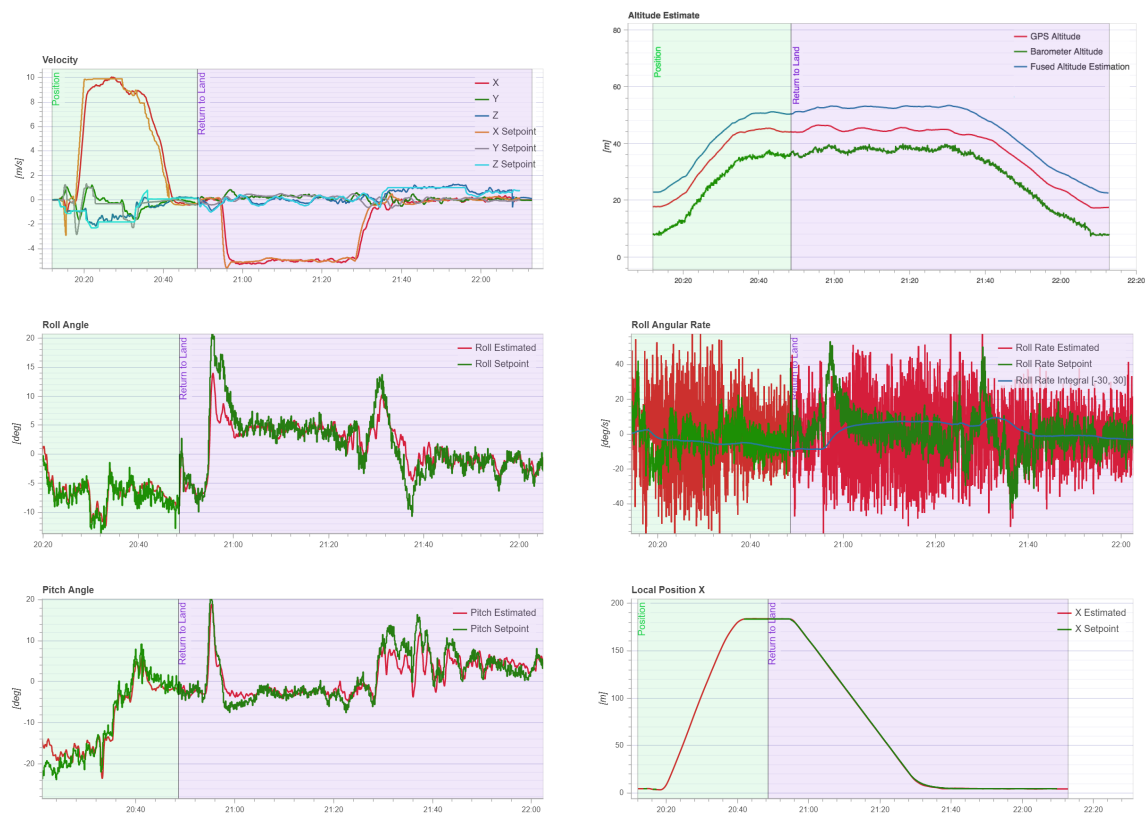
Figure 11. Plots of the velocity, attitude, and altitude over time during the landing procedure.

6. Conclusion and Future Work

This paper demonstrates a quadrotor helicopter landing control procedure through an RBFNN-based backstepping control approach. First, a soft landing gear is designed that effectively absorbs the landing impact force. Second, an RBFNN-based backstepping control system is designed for the quadrotor helicopter. Third, a Lyapunov analysis is used to prove the stability of the proposed control system with external disturbances and uncertainties.

The soft landing gear and the RBFNN-based backstepping control methods work together to render the quadrotor helicopter system able to softly and precisely land on a challenging, non-flat surface. The effectiveness of the proposed RBFNN-based backstepping control strategy was further tested in field experiments. Future work will focus on enabling the quadrotor UAV to detect and choose the landing zone autonomously, without the support of GPS.

Author Contributions: Conceptualization, C.L.; Data curation, L.Y.; Funding acquisition, C.L.; Methodology, C.L.; Software, W.Z. and L.Y.; Visualization, W.Z.; Writing—original draft, C.L.; Writing—review & editing, C.L., Z.D., and L.Y.

Conflicts of Interest: The authors declare no conflict of interest.

References

1. Ding, X.; Yu, Y. Motion Planning and Stabilization Control of a Multipropeller Multifunction Aerial Robot. *IEEE/ASME Trans. Mechatron.* **2013**, *18*, 645–656. [CrossRef]
2. Sun, W.; Gao, H.; Kaynak, O. Adaptive Backstepping Control for Active Suspension Systems with Hard Constraints. *IEEE/ASME Trans. Mechatron.* **2013**, *18*, 1072–1079. [CrossRef]

3. Rus, D.; Tolley, M.T. Design, fabrication and control of soft robots. *Nature* **2015**, *521*, 467. [CrossRef] [PubMed]

4. Omari, S.; Hua, M.D.; Ducard, G.; Hamel, T. Hardware and Software Architecture for Nonlinear Control of Multirotor Helicopters. *IEEE/ASME Trans. Mechatron.* **2013**, *18*, 1724–1736. [CrossRef]

5. Zhang, G.; He, Y.; Dai, B.; Gu, F.; Yang, L.; Han, J.; Liu, G. Aerial Grasping of an Object in the Strong Wind: Robust Control of an Aerial Manipulator. *Appl. Sci.* **2019**, *9*, 2230. [CrossRef]

6. Lee, D.; Franchi, A.; Son, H.I.; Ha, C.; Bülthoff, H.H.; Giordano, P.R. Semiautonomous Haptic Teleoperation Control Architecture of Multiple Unmanned Aerial Vehicles. *IEEE/ASME Trans. Mechatron.* **2013**, *18*, 1334–1345. [CrossRef]

7. Johnson, A.; Montgomery, J.; Matthies, L. Vision Guided Landing of an Autonomous Helicopter in Hazardous Terrain. In Proceedings of the IEEE International Conference on Robotics and Automation (ICRA), Barcelona, Spain, 18–22 April 2005.

8. Templeton, T.; Shim, D.H.; Geyer, C.; Sastry, S.S. Autonomous Vision-based Landing and Terrain Mapping Using an MPC-controlled Unmanned Rotorcraft. In Proceedings of the IEEE International Conference on Robotics and Automation (ICRA), Roma, Italy, 10–14 April 2007.

9. Kendoul, F. Survey of advances in guidance, navigation, and control of unmanned rotorcraft systems. *J. Field Robot.* **2012**, *29*, 315–378. [CrossRef]

10. Barton, J.D. A Biologically-Inspired Micro Aerial Vehicle—Sensing, Modeling and Control Strategies. *Johns Hopkins APL Tech. Dig.* **2012**, *31*, 153–178.

11. Bosch, S.; Lacroix, S.; Caballero, F. Autonomous Detection of Safe Landing Areas for an UAV from Monocular Images. In Proceedings of the IEEE/RSJ International Conference on Intelligent Robots and Systems (IROS), Beijing, China, 9–15 October 2006.

12. Scherer, S.; Chamberlain, L.; Singh, S. Autonomous landing at unprepared sites by a full-scale helicopter. *Robot. Auton. Syst.* **2012**, *60*, 1545–1562. [CrossRef]

13. Brockers, R.; Bouffard, P.; Ma, J.; Matthies, L.; Tomlin, C. Autonomous landing and ingress of micro-air-vehicles in urban environments based on monocular vision. In Proceedings of the SPIE 8031, Micro- and Nanotechnology Sensors, Systems, and Applications III, Orlando, FL, USA, 25–29 April 2011.

14. Cory, R.; Tedrakey, R. Experiments in Fixed-Wing UAV Perching. In Proceedings of the AIAA Guidance, Navigation and Control Conference and Exhibit, Honolulu, HI, USA, 18–21 August 2008.

15. Zhang, K.; Chermprayong, P.; Tzoumanikas, D.; Li, W.; Grimm, M.; Smentoch, M.; Leutenegger, S.; Kovac, M. Bioinspired design of a landing system with soft shock absorbers for autonomous aerial robots. *J. Field Robot.* **2019**, *36*, 230–251. [CrossRef]

16. Desbiens, A.L.; Asbeck, A.T.; Cutkosky, M.R. Landing, perching and taking off from vertical surfaces. *Int. J. Robot. Res.* **2011**, *30*, 355–370. [CrossRef]

17. Doyle, C.E.; Bird, J.J.; Isom, T.A.; Johnson, C.J.; Kallman, J.C.; Simpson, J.A.; King, R.J.; Abbott, J.J.; Minor, M.A. Avian-inspired passive perching mechanism for robotic rotorcraft. In Proceedings of the IEEE/RSJ International Conference on Intelligent Robots and Systems (IROS), San Francisco, CA, USA, 25–30 September 2011.

18. Nguyen, H.N.; Siddall, R.; Stephens, B.; Navarro-Rubio, A.; Kovač, M. A Passively Adaptive Microspine Grapple for Robust, Controllable Perching. In Proceedings of the 2019 2nd IEEE International Conference on Soft Robotics (RoboSoft), Seoul, Korea, 14–18 April 2019; pp. 80–87.

19. Liang, X.; Fang, Y.; Sun, N.; Lin, H. Nonlinear hierarchical control for unmanned quadrotor transportation systems. *IEEE Trans. Ind. Electron.* **2017**, *65*, 3395–3405. [CrossRef]

20. Qian, L.; Liu, H.H. Path Following Control of A Quadrotor UAV with A Cable Suspended Payload Under Wind Disturbances. *IEEE IEEE Trans. Ind. Electron.* **2019**. [CrossRef]

21. Alexis, K.; Nikolakopoulos, G.; Tzes, A. Switching model predictive attitude control for a quadrotor helicopter subject to atmospheric disturbances. *Control Eng. Pract.* **2011**, *19*, 1195–1207. [CrossRef]

22. Wang, L.; Su, J. Robust disturbance rejection control for attitude tracking of an aircraft. *IEEE Trans. Control Syst. Technol.* **2015**, *23*, 2361–2368. [CrossRef]

23. Benallegue, A.; Mokhtari, A.; Fridman, L. High-order sliding-mode observer for a quadrotor UAV. *Int. J. Robust Nonlinear Control IFAC-Affil. J.* **2008**, *18*, 427–440. [CrossRef]

24. Ordaz, J.; Salazar, S.; Mondié, S.; Romero, H.; Lozano, R. Predictor-based position control of a quad-rotor with delays in GPS and vision measurements. *J. Intell. Robot. Syst.* **2013**, *70*, 13–26. [CrossRef]

25. Wang, Q.; Wang, J.W.; Yu, Y.; Sun, C.Y. Robust attitude control of an indoor micro quadrotor with input delay. In Proceedings of the 2014 IEEE Chinese Guidance, Navigation and Control Conference, Yantai, China, 8–10 August 2014; pp. 2363–2368.

26. Rosales, C.; Soria, C.M.; Rossomando, F.G. Identification and adaptive PID Control of a hexacopter UAV based on neural networks. *Int. J. Adapt. Control Signal Process.* **2019**, *33*, 74–91. [CrossRef]

27. Furukawa, S.; Kondo, S.; Takanishi, A.; Lim, H.O. Radial basis function neural network based PID control for quad-rotor flying robot. In Proceedings of the 2017 17th International Conference on Control, Automation and Systems (ICCAS), Jeju, Korea, 18–21 October 2017; pp. 580–584.

28. Kantue, P.; Pedro, J.O. Nonlinear Identification of an Unmanned Quadcopter Rotor Dynamics using RBF Neural Networks. In Proceedings of the 2018 22nd International Conference on System Theory, Control and Computing (ICSTCC), Sinaia, Romania, 10–12 October 2018; pp. 292–298.

29. Bouabdallah, S.; Siegwart, R. Full control of a quadrotor. In Proceedings of the 2007 IEEE/RSJ International Conference on Intelligent Robots and Systems, San Diego, CA, USA, 29 October–2 November 2007; pp. 153–158.

30. Tayebi, A.; McGilvray, S. Attitude stabilization of a VTOL quadrotor aircraft. *IEEE Trans. Control Syst. Technol.* **2006**, *14*, 562–571. [CrossRef]

31. Sun, J.; Wang, Y.; Yu, Y.; Sun, C. Nonlinear Robust Compensation Method for Trajectory Tracking Control of Quadrotors. *IEEE Access* **2019**. [CrossRef]

32. Hoffmann, G.; Huang, H.; Waslander, S.; Tomlin, C. Quadrotor helicopter flight dynamics and control: Theory and experiment. In Proceedings of the AIAA Guidance, Navigation and Control Conference and Exhibit, Hilton Head, SC, USA, 20–23 August 2007; p. 6461.

33. Tran, D.T.; Nguyen, M.N.; Ahn, K.K. RBF Neural Network Based Backstepping Control for an Electrohydraulic Elastic Manipulator. *Appl. Sci.* **2019**, *9*, 2237. [CrossRef]

34. Ge, S.S.; Hang, C.C.; Lee, T.H.; Zhang, T. *Stable Adaptive Neural Network Control*; Springer Science & Business Media: Berlin, Germany, 2013; Volume 13.

35. He, W.; Chen, Y.; Yin, Z. Adaptive neural network control of an uncertain robot with full-state constraints. *IEEE Trans. Cybern.* **2016**, *46*, 620–629. [CrossRef] [PubMed]

36. Peng, C.; Bai, Y.; Gong, X.; Gao, Q.; Zhao, C.; Tian, Y. Modeling and robust backstepping sliding mode control with Adaptive RBFNN for a novel coaxial eight-rotor UAV. *IEEE/CAA J. Autom. Sin.* **2015**, *2*, 56–64.

37. Slotine, J.J.E.; Li, W. *Applied Nonlinear Control*; Prentice Hall: Englewood Cliffs, NJ, USA, 1991; Volume 199.

38. Meier, L.; Tanskanen, P.; Fraundorfer, F.; Pollefeys, M. Pixhawk: A system for autonomous flight using onboard computer vision. In Proceedings of the 2011 IEEE International Conference on Robotics and Automation, Shanghai, China, 9–13 May 2011; pp. 2992–2997.

39. Meier, L.; Tanskanen, P.; Heng, L.; Lee, G.H.; Fraundorfer, F.; Pollefeys, M. PIXHAWK: A micro aerial vehicle design for autonomous flight using onboard computer vision. *Auton. Robot.* **2012**, *33*, 21–39. [CrossRef]

40. Marty, J.A. *Vulnerability Analysis of the Mavlink Protocol for Command and Control of Unmanned Aircraft*; Technical Report; Graduate School of Engineering and Management, Air Force Institute of Technology: Wright-Patterson AFB, OH, USA, 2013.